

Molecular movie of ultrafast coherent rotational dynamics

Evangelos T. Karamatskos,^{1,2} Sebastian Raabe,³ Terry Mullins,¹ Andrea Trabattoni,^{1,2}
Philipp Stammer,³ Gildas Goldsztejn,³ Rasmus R. Johansen,⁴ Karol Długołęcki,¹ Henrik Stapelfeldt,⁴
Marc J. J. Vrakking,³ Sebastian Trippel,^{1,5} Arnaud Rouzée,^{3,||} and Jochen Küpper^{1,2,5,*}

¹Center for Free-Electron Laser Science, Deutsches Elektronen-Synchrotron DESY, Notkestraße 85, 22607 Hamburg, Germany

²Department of Physics, Universität Hamburg, Luruper Chaussee 149, 22761 Hamburg, Germany

³Max Born Institute, Max-Born-Straße 2a, 12489 Berlin, Germany

⁴Department of Chemistry, Aarhus University, Langelandsgade 140, 8000 Aarhus C, Denmark

⁵The Hamburg Center for Ultrafast Imaging, Universität Hamburg, Luruper Chaussee 149, 22761 Hamburg, Germany

Recording molecular movies on ultrafast timescales has been a longstanding goal for unravelling detailed information about molecular dynamics. We present the direct experimental recording of very-high-resolution and -fidelity molecular movies over more than one-and-a-half periods of the laser-induced rotational dynamics of carbonylsulfide (OCS) molecules. Utilising the combination of single quantum-state selection and an optimised two-pulse sequence to create a tailored rotational wavepacket, an unprecedented degree of field-free alignment, $\langle \cos^2\theta_{2D} \rangle = 0.96$ ($\langle \cos^2\theta \rangle = 0.94$) was achieved, exceeding the theoretical limit for single-pulse alignment. The very rich experimentally observed quantum dynamics is fully recovered by the angular probability distribution obtained from solutions of the time-dependent Schrödinger equation with parameters refined against the experiment. The populations and phases of rotational states in the retrieved time-dependent three-dimensional wavepacket rationalised the observed very high degree of alignment.

The filming of nuclear motion during molecular dynamics at relevant timescales, dubbed the “molecular movie”, has been a longstanding dream in the molecular sciences [1, 2]. Recent experimental advances with x-ray-free-electron lasers and ultrashort-pulse electron guns have provided first glimpses of intrinsic molecular structures [3–5] and dynamics [2, 6, 7]. However, despite the spectacular progress, the fidelity of the recorded movies, in comparison to the investigated dynamics, was limited so far. Especially for high-precision studies of small molecules, typically only distances between a few atoms were determined [4, 5, 7].

Rotational quantum dynamics of isolated molecules provides an interesting and important testbed that provides and requires direct access to angular coordinates. Furthermore, different from most molecular processes, it can be practically exactly described by current numerical methods, even for complex molecules. Rotational wavepackets were produced through the interaction of the molecule with short laser pulses [8–10], which couple different rotational states through stimulated Raman transitions. The resulting dynamics were observed, for instance, by time-delayed Coulomb-explosion ion imaging [9, 11, 12], photoelectron imaging [13], or ultrafast electron diffraction [14]. The rotational wavepackets were exploited to connect the molecular and laboratory frames through strong-field alignment [9, 10] and mixed-field orientation [15, 16], as well as for the determination of molecular-structure information in rotational-coherence spectroscopy [17, 18]. Coherent rotational wavepacket manipulation using multiple pulses [19] or appropriate turn-on and -off timing [20] allowed enhanced or diminished rephasing, and it was suggested as a realisation of quantum computing [19]. Furthermore, methods for rotational-wavepacket recon-

struction of linear molecules [21] and for benzene [22] were reported.

Here, we demonstrate the direct experimental high-resolution imaging of the time-dependent angular probability-density distribution of a rotational wavepacket and its reconstruction in terms of the populations and phases of field-free rotor states. Utilising a state-selected molecular sample and an optimised two-laser-pulse sequence, a broad phase-locked rotational wavepacket was created. Using mid-infrared-laser strong-field ionisation and Coulomb-explosion ion imaging, an unprecedented degree of field-free alignment of $\langle \cos^2\theta_{2D} \rangle = 0.96$, or $\langle \cos^2\theta \rangle = 0.94$, was obtained at the full revivals, whereas in between a rich angular dynamics was observed with very high resolution, from which the complete wavepacket could be uniquely reconstructed. While the dynamics has low dimensionality, The resulting — purely experimentally obtained — movie provides a most direct realisation of the envisioned “molecular movie”. We point out that the data also is a measurement of a complete quantum carpet [23].

In order to achieve such a high degree of alignment, better than the theoretical maximum of $\langle \cos^2\theta \rangle = 0.92$ for single-pulse alignment [24, 25], we performed a pump-probe experiment with ground-state-selected OCS molecules [26], with > 80 % purity, as a showcase. Two off-resonant near-IR pump pulses of 800 nm central wavelength, separated by 38.1 (1) ps and with a pulse duration of 250 fs, i. e., much shorter than the rotational period of OCS of 82.2 ps, were used to create the rotational wavepacket. These pulses were linearly polarised parallel to the detector plane. The probe pulse with a central wavelength of 1.75 μm was polarised perpendicularly to the detector plane to minimise the effects of geometric

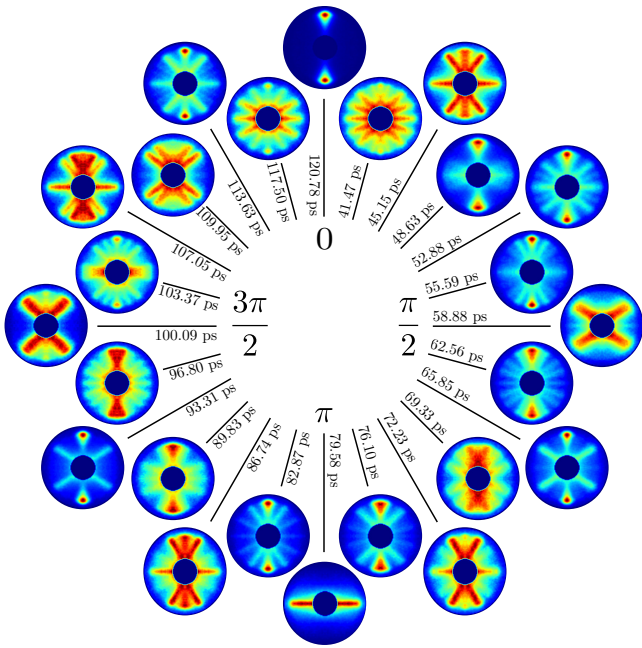


FIG. 1. **Rotational clock depicting the molecular movie of the observed quantum dynamics.** Individual experimental VMI images of O^+ ion-momentum distributions depicting snapshots of the rotational wavepacket over one full period. The displayed data was recorded from the first (prompt) revival at 38.57 ps (0) to the first full revival at 120.78 ps (2π); the phase-evolution of $\pi/12$ between images corresponds to ~ 3.43 ps and the exact delay times of the individual images are specified. Full movies are available as part of the Supplementary Information.

alignment and ensures that the observed degree of alignment was a lower boundary of the real value. The probe pulse multiply ionised the molecules, resulting in Coulomb explosion into ionic fragments. 2D ion-momentum distributions of O^+ fragments, which reflect the orientation of the molecules in space at the instance of ionisation, were recorded by a velocity map imaging (VMI) spectrometer [27] for different time delays between the alignment pulse sequence and the probe pulse. Further details of the experimental setup are presented in *Methods*.

In Fig. 1 snapshots of the experimentally recorded molecular movie, i. e., 2D ion-momentum distributions, are shown for several probe times covering a whole rotational period. The phase of 0 and 2π correspond to $t = 38.57$ ps and 120.78 ps after the peak of the first alignment laser pulse at $t = 0$, respectively. The simplest snapshot-images, reflecting an unprecedented degree of field-free alignment $\langle \cos^2\theta_{2D} \rangle = 0.96$, were obtained for the alignment revivals at phases of 0 and 2π , which correspond to the prompt alignment and its revival regarding the second laser pulse. Here, the molecular axes are preferentially aligned along the alignment-laser polarisation. For the anti-alignment at a phase of π the

molecules are preferentially aligned in a plane perpendicular to the alignment laser polarisation direction. Simple quadrupolar structures are observed at $\pi/2$ and $3\pi/2$. At intermediate times, e. g., at $\pi/3$ or $7\pi/12$, the images display rich angular structures, which could be observed due to the high angular experimental resolution of the recorded movie, which is 4° as derived in the Supplementary Information. This rich structure directly reflects the strongly quantum-state selected initial sample exploited in these measurements, whereas the structure would be largely lost in the summation of wavepackets from even a few initially populated states.

The dynamics was analysed as follows: Through the interaction of the molecular ensemble with the alignment laser pulses, a coherent wavepacket was created from each of the initially populated rotational states. These wavepackets were expressed as a coherent superposition of eigenfunctions of the field-free rotational Hamiltonian, i. e.,

$$\Psi(\theta, \phi, t) = \sum_J a_J(t) Y_J^M(\theta, \phi), \quad (1)$$

with the time-dependent complex amplitudes $a_J(t)$, the spherical harmonics $Y_J^M(\theta, \phi)$, the quantum number of angular momentum J , and its projection M onto the laboratory-fixed axis defined by the laser polarisation. We note that M was conserved and thus no ϕ dependence existed. The angular distribution is defined as the sum of the squared moduli of all $\Psi(\theta, \phi, t)$ weighted by the initial-state populations.

The degree of alignment was extracted from the VMI images using the commonly utilised expectation value $\langle \cos^2\theta_{2D} \rangle$. The maximum value observed at the alignment revival reached 0.96, which, to the best of our knowledge, is the highest degree of field-free alignment achieved to date. Comparing the angular distributions at different delay times with the degree of alignment $\langle \cos^2\theta_{2D} \rangle$, see Fig. S4 in the Supplementary Information, we observed the same degree of alignment for angular distributions that are in fact very different from each other. This highlights that much more information is contained in the angular distributions than in the commonly utilised expectation value [10]. Indeed, $\langle \cos^2\theta_{2D} \rangle$ merely describes the leading term in an expansion of the angular distribution, for instance, in terms of Legendre polynomials, see (1) in the Supplementary Information. In order to fully characterise the angular distribution a description in terms of a polynomial series is necessary that involves the same maximum order as the maximum angular momentum J_{\max} of the populated rotational eigenstates, which corresponds to, at most, $2J_{\max}$ lobes in the momentum maps.

As the probe laser is polarised perpendicularly to the detector plane, the cylindrical symmetry as generated by the alignment-laser polarisation was broken and an Abel inversion to retrieve the 3D angular distribution directly

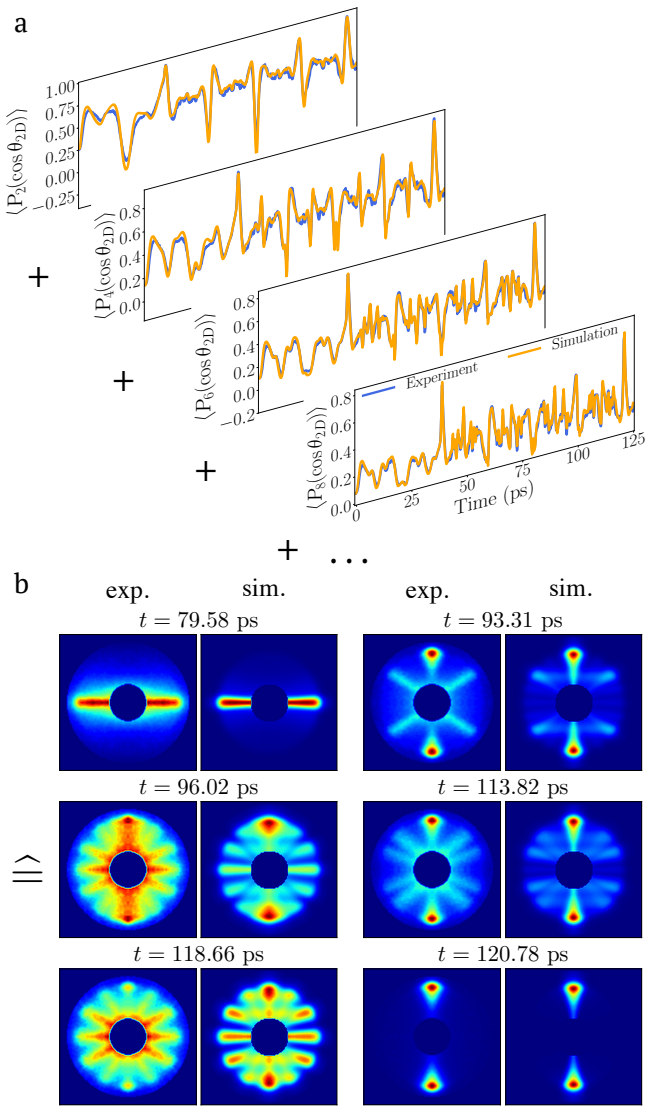


FIG. 2. **Decomposition of angular distributions into their moments.** **a** Comparison of the decomposition of the experimental and theoretical angular distributions in terms of Legendre polynomials. **b** Simulated and experimental angular-distribution VMI images for selected times; the radial distributions in the simulations are extracted from the experimental distribution at 120.78 ps, see text for details.

from the experimental VMI images was not possible. In order to retrieve the complete 3D wavepacket, the time-dependent Schrödinger equation (TDSE) was solved for a rigid rotor coupled to a non-resonant ac electric field representing the two laser pulses as well as the dc electric field of the VMI spectrometer. For a direct comparison with the experimental data the rotational wavepacket and thus the 3D angular distribution was constructed and, using a Monte-Carlo approach, projected onto a 2D screen using the radial distribution extracted from the experiment at the alignment revival at 120.78 ps. The relation between the 3D rotational wavepacket and the 2D projected

density is graphically illustrated in Fig. S2 of the Supplementary Information. The anisotropic angle-dependent ionisation efficiency for double ionisation, resulting in a two-body breakup into O^+ and CS^+ fragments, was taken into account by approximating it by the square of the measured single-electron ionisation rate. Non-axial recoil during the fragmentation process is expected to be negligible and was not included in the simulations.

The initial state distribution in the quantum-state selected OCS sample as well as the interaction volume with the alignment and probe lasers were not known *a priori* and used as fitting parameters. For each set of parameters the TDSE was solved and the 2D projection of the rotational density, averaged over the initial state distribution and the interaction volume of the pump and probe lasers, was carried out. The aforementioned expansion in terms of Legendre polynomials was realised for the experimental and simulated angular distributions and the best fit was determined through least squares minimisation, see Supplementary Information. Taking into account the eight lowest even moments of the angular distribution allowed to precisely reproduce the experimental angular distribution. The results for the first four moments are shown in Fig. 6 a; the full set is given in Fig. S3 in the Supplementary Information as well as the optimal fitting parameters. The overall agreement between experiment and theory is excellent for all moments. Before the onset of the second pulse, centred around $t = 38.1$ ps, the oscillatory structure in all moments is fairly slow compared to later times, which reflects the correspondingly small number of interfering states in the wavepacket before the second pulse, and the large number thereafter.

Theoretical images, computed for the best fit parameters, are shown in Fig. 6 b; a full movie is provided with the Supplementary Information. The theoretical results are in excellent agreement with the measured ion-momentum angular distributions at all times, see Supplementary Information, and prove that we were able to fully reconstruct the 3D rotational wavepacket with the amplitudes and phases of all rotational states included.

In Fig. 3 a, the extracted rotational-state populations are shown for the wavepacket created from the rotational ground state after the first and the second alignment laser pulse. It clearly shows that the rotational-state distribution is broader after the second pulse, reaching up to $J \geq 16$. This also matches the convergence of the Legendre-polynomial series, with eight even terms, derived from the fit to the data above. In Fig. 3 b the corresponding phase differences for all populated states relative to the initial state with the largest population in the wavepacket are shown, where $\phi(J)$ is the phase of the complex coefficient a_J in (1). Combining these populations and phases it became clear that the very high degree of alignment after the second alignment pulse arises from the combination of the broad distribution of rotational states, reaching large angular momenta, and

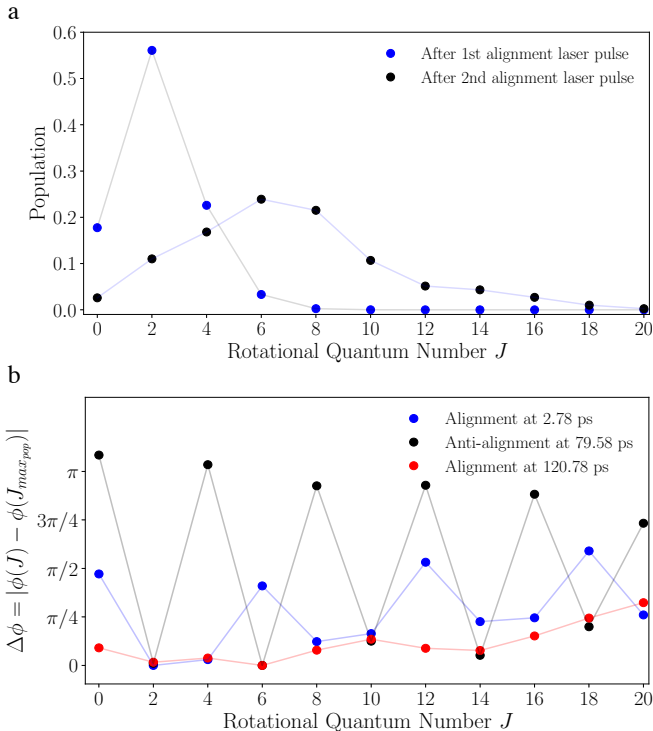


FIG. 3. Populations and phase differences in the rotational wavepacket at alignment and anti-alignment times

a Rotational-state populations and **b** phase-differences to the phase of the state with largest population, $J = 2$, $J = 6$, respectively, at the alignment revival following a single-pulse excitation, 2.78 ps (blue dots), and the two-pulse excitation, 120.78 ps (red dots) as well as for the anti-alignment at 79.58 ps (black dots, populations coincide with the red dots). Only states with even angular momentum are populated due to the Raman-transition selection rules $\Delta J = \pm 2$.

the very strong and flat rephasing of all significantly populated states at the revival at 120.78 ps, Fig. 3 b (red). Similarly, the anti-alignment at 79.58 ps occurs due to alternating phase differences of π between adjacent populated rotational states, Fig. 3 b (black).

In conclusion, we were able to record a high-resolution molecular movie of the ultrafast coherent rotational motion of impulsively aligned OCS molecules. State-selection and an optimised two-pulse sequence yielded an unprecedented degree of field-free alignment of $\langle \cos^2\theta_{2D} \rangle = 0.96$, with a very narrow angular confinement of 13.4° FWHM. Limiting the analysis to a determination of $\langle \cos^2\theta_{2D} \rangle$, as it is common in experiments on time-dependent alignment, did not allow to capture the rich rotational dynamics, while the use of a polynomial expansion up to an appropriate order did. We reconstructed the rotational wavepacket, from which the complex coefficients and, hence, the full information about the rotational wavepacket under study was extracted. The 2D projection of the reconstructed rotational wavepacket allowed

a direct comparison with the experimentally measured data.

Regarding the extension toward the investigation of chemical dynamics, we point out that strong-field-ionisation-induced Coulomb-explosion imaging can be used, for instance, to image the configuration of chiral molecules [28] or internal torsional dynamics [29]. Following the dynamics of such processes with the detail and quality presented here would directly yield a molecular movie of the chemical and, possibly, chirality dynamics [30]. Furthermore, the very high degree of field-free alignment achieved here would be extremely useful for stereochemistry studies [31, 32] as well as for molecular-frame imaging experiments [4, 5, 14, 33–38].

METHODS

A cold molecular beam was formed by supersonic expansion of a mixture of OCS (500 ppm) in helium, maintained at a backing pressure of 90 bar from a pulsed Even-Lavie valve [39] operated at 250 Hz. After passing two skimmers, the collimated molecular beam entered the Stark deflector. The beam was dispersed according to quantum state by a strong inhomogeneous electric field [26] with a nominal strength of ~ 200 kV/cm. Through a movable third skimmer, the molecular beam entered the spectrometer. Here, it was crossed at right angle by laser beams, where the height of the laser beams allowed to probe state-selected molecular ensembles, i. e., a practically pure rovibronic-ground-state sample of OCS [16, 20, 40].

The laser setup consisted of a commercial Ti:Sapphire laser system (KM labs) delivering pulses with 30 mJ pulse energy, 35 fs (FWHM) pulse duration, and a central wavelength of 800 nm at a 1 kHz repetition rate. One part (20 mJ) of the laser output was used to pump a high-energy tunable optical parametric amplifier (HE-TOPAS, Light Conversion) to generate pulses with a central wavelength of $1.75 \mu\text{m}$, a pulse duration of 60 fs, and a pulse energy of ~ 1.5 mJ. 900 μJ of the remaining 800 nm laser output was used for the laser-induced alignment, i. e., the generation of the investigated rotational wavepackets. This beam was split into two parts with a 4:1 energy ratio using a Mach-Zehnder interferometer. A motorised delay stage in one beam path allowed for controlling the delay between the two pulses. This delay was optimised experimentally and maximum alignment was observed for $\tau_{exp} = 38.1 \pm 0.1$ ps, in perfect agreement with the theoretically predicted $\tau_{sim} = 38.2$ ps. The pulses were combined collinearly and passed through a 2 cm long SF₁₁ optical glass to stretch them to 250 fs pulse duration (FWHM). Then the alignment pulses were collinearly overlapped with the $1.75 \mu\text{m}$ mid-infrared pulses using a dichroic mirror. All pulses were focused into the velocity map imaging spectrometer (VMI) using a 25 cm focal-distance calcium fluoride lens.

At the center of the VMI the state-selected molecular beam and the laser beams crossed at right angle. Following strong-field multiple ionisation of the molecules, the generated charged fragments were projected by the VMI onto a combined multichannel-plate (MCP) phosphor-screen detector and read out by a CCD camera. The angular resolution of the imaging system is 4° , limited by the 1 megapixel camera, see Supplementary Information. 2D ion-momentum distributions of O^+ fragments were recorded as a function of the delay between the 800 nm pulses and the ionising $1.75 \mu\text{m}$ pulses in order to characterise the angular distribution of the molecules through Coulomb-explosion imaging. The polarisation of the 800 nm alignment pulses was parallel to the detector screen whereas that of the $1.75 \mu\text{m}$ ionising laser was perpendicular in order to avoid geometric-alignment effects in the angular distributions. For this geometry, unfortunately, it was not possible to retrieve 3D distributions from an inverse Abel transform. 651 images were recorded in steps of 193.4 fs, covering the time interval from -0.7 ps up to 125 ps, which is more than one and a half times the rotational period of OCS of 82.2 ps.

OPTIMISATION OF TWO-PULSE FIELD-FREE ALIGNMENT

Optimisation calculations were performed in order to predict the optimal pulse parameter for single and two-pulse field-free alignment. In the simulations, the rotational part of the Schrödinger equation for a linear rigid rotor within the Born-Oppenheimer approximation coupled to non-resonant ac alignment laser pulses and a static electric field, as provided by the VMI in the interaction region, was used. The Hamiltonian of the system is described in detail in reference [?]. The global differential-evolution-optimisation algorithm [?] was used to calculate the optimal alignment characterised through the expectation value $\langle \cos^2\theta \rangle$ in a closed-feedback-loop approach. The optimisation parameters used were the intensities and one common duration of Fourier-limited Gaussian pulses and the delay between the pulses in the case of two-pulse alignment. In the calculations a pure rotational ground state ensemble was assumed and no integration over the interaction volume was carried out. The former is justified as we know that the ground state contribution to alignment is dominant and the exact experimental conditions were not known a priori. Furthermore, exploiting the electrostatic deflector, as in our experiment, almost pure ground state ensembles can be prepared [26, 40]. Including also thermally excited rotational states lead to an additional incoherent sum over all states present in the initial distribution of rotational states and in general to a decrease of the degree of alignment. The same holds for the interaction volume of the laser since only molecules at the center of the beam experience the optimal alignment

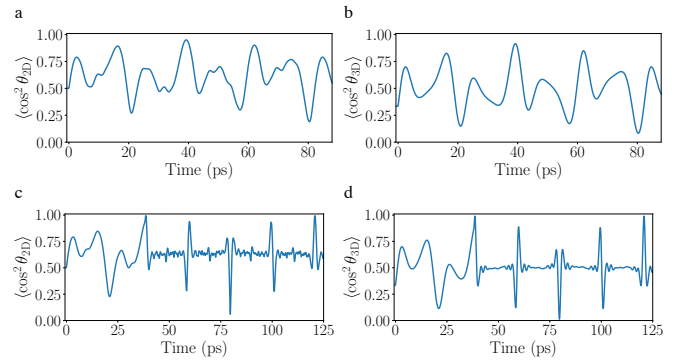


FIG. 4. Optimised **a, c** 2D and **b, d** 3D field-free alignment with **a, b** one and **c, d** two alignment pulses.

intensity while molecules at some distance from the center interact with a lower field. In this sense the calculated values constitute an upper limit for the alignment under optimal conditions. Time-evolution curves of the optimal two-dimensional (2D) and three-dimensional (3D) alignment are shown in Fig. 4. The results for the single pulse optimisation yielded a pulse duration of 114.5 fs and a maximum intensity of $5.6 \text{ TW}/\text{cm}^2$. The corresponding maximum degree of field-free 3D alignment was found to be $\langle \cos^2\theta \rangle = 0.92$, which is in agreement with an upper bound of 0.92 derived previously [25]; this corresponds to a 2D degree of alignment of $\langle \cos^2\theta_{2D} \rangle = 0.95$.

The optimal parameters for the case of two alignment pulses were found to be a pulse duration of 273.4 fs, a pulse separation between the two pulses of 38.2 ps, and an intensity-ratio of $\sim 1 : 5$ with the first pulse being weaker than the second one, in agreement with previous results [24?]. The maximum intensity of the first pulse was determined to be $1.93 \text{ TW}/\text{cm}^2$ and that of the second pulse $10 \text{ TW}/\text{cm}^2$, which was the upper bound of intensities included in the calculations since for higher values at a wavelength of 800 nm a non-negligible amount of ionisation of OCS sets in. The maximum degree of 3D field-free alignment calculated with these parameters were $\langle \cos^2\theta \rangle = 0.99$ and $\langle \cos^2\theta_{2D} \rangle = 0.99$, substantially higher than in the single pulse case. The experiment presented in the main paper was performed under experimental conditions approximating these optimised parameter. We note that the optimal pulse separation was calculated to be 38.2 ps, which was confirmed in the experiment, for which a scan of the pulse separation yielded the best alignment revival for 38.1 ± 0.1 ps.

MOMENTS OF ANGULAR DISTRIBUTION

There are several ways to expand the angular distribution of the wavepacket in a power series [?], but a natural basis consists of the Legendre polynomials, as for $\Delta M = 0$ the eigenstates are independent of ϕ and the spherical

harmonics simplify to Legendre polynomials. Only even order polynomials appear in the expansion since for a ground-state-selected ensemble the odd order moments describe orientation of the molecular axes, which was not present. The expansion takes on the form

$$P(\theta_{2D}, t) = \sum_{k=0, k \text{ even}}^{J_{\max}} a_k(t) \mathcal{P}_k(\cos \theta_{2D}) \quad (2)$$

where the full time-dependent angular distribution is denoted as $P(\theta_{2D}, t)$ and a_k ($k = 0, 2 \dots J_{\max}$) are the expansion coefficients corresponding to the k -th Legendre polynomial \mathcal{P}_k ; J_{\max} is the angular momentum quantum number of the highest populated rotational state in the wavepacket.

In order to characterise the initial state distribution of rotational states in the molecular beam, the eight lowest even-order moments of the experimental angular distributions were fitted simultaneously using least squares minimisation. For each moment, squared differences were summed according to

$$\chi_n^2 = \sum_t (\langle \mathcal{P}_{2n}(\cos \theta_{2D})_{\text{exp}} \rangle(t) - \langle \mathcal{P}_{2n}(\cos \theta_{2D})_{\text{sim,vol}} \rangle(t))^2, \quad (3)$$

where the sum runs over all measured delay times t and $n = 1 \dots 8$. In order to compute $\langle \mathcal{P}_n(\cos \theta_{2D})_{\text{sim,vol}} \rangle(t)$, several steps were followed. First, the coherent wavepackets, created through the interaction with the alignment laser pulses, were for every initial state described in the basis of field-free eigenstates as

$$\Psi_{J_i, M_i}(\theta, \phi, t) = \sum_J a_J(t) Y_J^{M_i}(\theta, \phi), \quad a_J(t=0) = \delta_{JJ_i}, \quad (4)$$

where $a_J(t) = |a_J(t)| e^{i\phi_J(t)}$ are time-dependent complex coefficients with amplitude $|a_J(t)|$, phase $\phi_J(t)$, and initial condition $a_J(t=0) = \delta_{JJ_i}$, δ_{JJ_i} is the Kronecker delta, obtained from the solution of the time-dependent Schrödinger equation; $Y_J^M(\theta, \phi)$ are the spherical-harmonic functions and J_i, M_i are the quantum numbers of the initial state from which the wavepacket is formed. The sum runs only over J , since M was a good quantum number due to cylindrical symmetry, as imposed by the linear polarisation of the alignment laser, and, hence, $\Delta M = 0$ and $M = M_i$ was conserved. Furthermore, the selection rules for transitions between different rotational states were $\Delta J = \pm 2$, since the population transfer is achieved via non-resonant two-photon Raman transitions. Moreover, the static VMI field was perpendicular to the alignment laser polarisation and does not mix different M states. Since more than one rotational state were initially populated, the 3D rotational density was obtained through the incoherent average with statistical weights w_{J_i, M_i}

$$P_{\text{sim,3D}}(\theta, \phi, t) = \sum_{J_i, M_i} w_{J_i, M_i} p(\theta) |\Psi_{J_i, M_i}(\theta, \phi, t)|^2, \quad (5)$$

which were not known *a priori* and used as fitting parameters. The function $p(\theta)$ describes the angle-dependent ionisation probability, which was approximated through the square of the measured angular-dependent single-electron ionisation rate. Finally, a focal average over the interaction region with the alignment and probe laser beam profiles, assumed to be Gaussian, was performed. The average over intensities in the laser focus was calculated through integration

$$\begin{aligned} \langle P_{\text{sim,3D}}(\theta, \phi, t) \rangle_{\text{vol}}(t) &= \\ &= \frac{1}{N} \int_0^{r_{\max}} \langle P_{\text{sim,3D}}(\theta, \phi, I_{\text{align}}(r), t) \rangle e^{-2r^2/w_{\text{probe}}^2} r dr \end{aligned} \quad (6)$$

with radius r_{\max} at $I_{\text{align}} = 10^9$ W/cm² and N a normalisation factor. The dependence of the rotational wavepackets on the alignment laser intensities is explicitly stated in (6). The widths of the laser beams were also not known *a priori* and were included as further fitting parameters. The resulting focal- and initial-state-averaged 3D rotational densities were projected onto a 2D plane using a Monte-Carlo sampling routine, which included the experimental radial distribution extracted at the full revival at a delay time of 120.78 ps, yielding the simulated VMI images in Fig. 2 in the main paper. The relation between the 3D rotational density and the 2D projected density is graphically illustrated in Fig. 5. The Legendre moments of the angular distribution were then extracted from the 2D projected images and compared to experiment through χ_n^2 , as described in (3). The statistical weights w_{J_i, M_i} of the initial state distribution and the laser focal sizes were varied until $\sum_n \chi_n^2$ converged to its minimum. The individual populations determined through the fitting procedure are $w_{00} = 8.2 \cdot 10^{-1}$, $w_{10} = 3.7 \cdot 10^{-2}$,

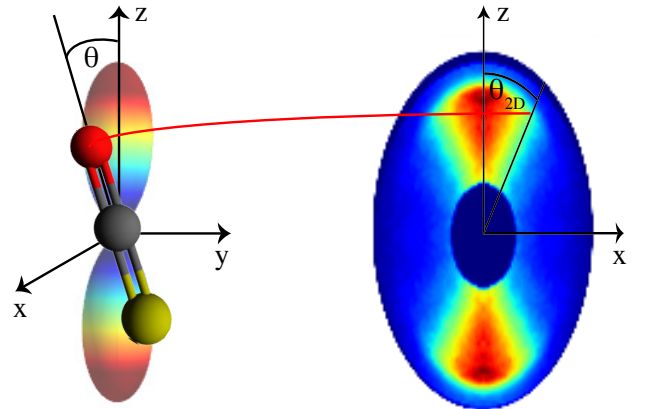


FIG. 5. Relation between the Euler angle θ , defining the alignment of the molecular axis with respect to the pump laser polarisation axis, and θ_{2D} , corresponding to the angle between the pump laser polarization and the detected ion-momentum distribution on the 2D detector.

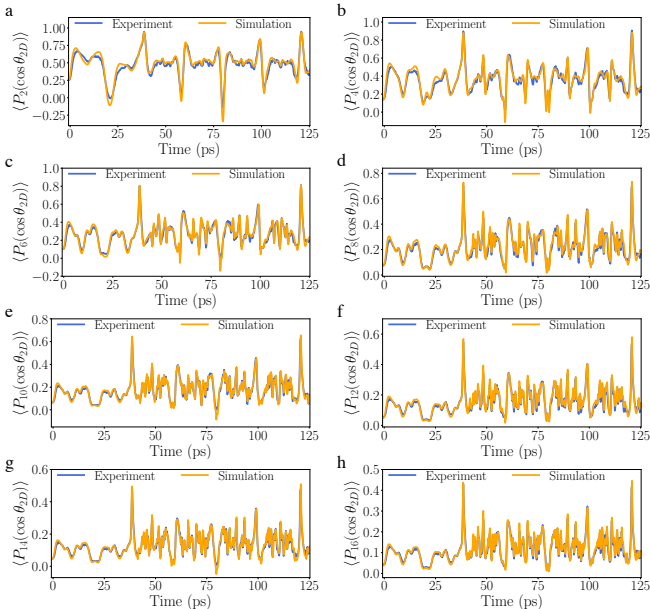


FIG. 6. Even order moments 1 to 8 of the angular distribution **a** $\langle P_2(\cos \theta_{2D}) \rangle$, **b** $\langle P_4(\cos \theta_{2D}) \rangle$, **c** $\langle P_6(\cos \theta_{2D}) \rangle$, **d** $\langle P_8(\cos \theta_{2D}) \rangle$ **e** $\langle P_{10}(\cos \theta_{2D}) \rangle$, **f** $\langle P_{12}(\cos \theta_{2D}) \rangle$, **g** $\langle P_{14}(\cos \theta_{2D}) \rangle$, **h** $\langle P_{16}(\cos \theta_{2D}) \rangle$.

$w_{11} = 7.5 \cdot 10^{-2}$, $w_{20} = 1.5 \cdot 10^{-2}$, $w_{21} = 2.1 \cdot 10^{-2}$ and $w_{22} = 3.2 \cdot 10^{-2}$ and the optimal focal parameter were determined to be $w_{\text{align}} = 130 \mu\text{m}$ for the alignment laser and $w_{\text{probe}} = 60 \mu\text{m}$ for the probe laser. The results are consistent with the fact that the probe laser was tighter focused than the alignment laser such that only molecules exhibiting strong alignment, close to the beam center, are probed.

The final results of the fitting procedure are shown in Fig. 2 in the main paper and in Fig. 6. The simulated angular distributions and the moments of the angular distribution are in excellent agreement with the experiment, in particular all oscillations are correctly captured, even for the highest-order moments. The experimental parameters used for the simulations were the peak intensities for the two alignment pulses of $I_{\text{align},1} = 1.92 \cdot 10^{12} \text{ W/cm}^2$ and $I_{\text{align},2} = 5.5 \cdot 10^{12} \text{ W/cm}^2$, the pulse duration of the alignment laser pulses $\tau_{\text{align}} = 255 \text{ fs}$, the time delay between the two alignment laser pulses $\tau_{\text{delay}} = 38.1 \text{ ps}$, and the pulse duration of the probe laser $\tau_{\text{probe}} = 60 \text{ fs}$. Calculations with 21 initial states, i. e., $J = 0 \dots 5, M = 0 \dots 5$, included in the initial rotational state distribution were originally performed, but convergence was already reached for the 6 lowest-energy states and the fitting procedure was restricted to using these 6 lowest rotational states, i. e., $J = 0 \dots 2, M = 0 \dots 2$, and the focal volume was averaged over 100 intensities in $I_{\text{align}} = 1 \cdot 10^9 \dots 5.5 \cdot 10^{12} \text{ W/cm}^2$. In all calculations the basis for each coherent wavepacket included all rotational states up to $J = 50$.

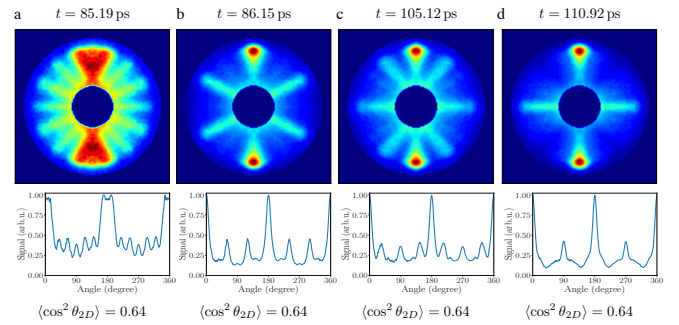


FIG. 7. Four O^+ ion momentum probability distributions recorded at different time delays, displaying very different angular distributions, but having all the same degree of alignment of $\langle \cos^2 \theta_{2D} \rangle = 0.64$. These distributions were recorded for delay times of **a** 85.19 ps, **b** 86.15 ps, **c** 105.12 ps, and **d** 110.92 ps.

ANGULAR DISTRIBUTIONS

As pointed out in the main text, we observed angular probability distributions showing the very rich time evolution of the rotational wavepacket created by the two alignment laser pulses. When characterising the degree of alignment using the commonly used $\langle \cos^2 \theta_{2D} \rangle$ we observed that completely different angular distributions possess the same degree of alignment, which pointed out the need for higher order terms in the expansion of the total angular distribution, e. g., in the basis of Legendre polynomials, to be able to reconstruct the complete rotational wavepacket. In Fig. 7 we present O^+ ion momentum distributions measured at four different delay times together with their corresponding angular distributions corroborating this observation. The delay times were chosen such that all distributions have the same $\langle \cos^2 \theta_{2D} \rangle = 0.64$, corresponding to the permanent alignment level. Although the degree of alignment is quite low compared to the maximum degree of alignment achieved, one clearly sees in particular in Fig. 7 b–d that nevertheless there is a substantial amount of molecules being strongly aligned. Thus it is clearly not sufficient to just use the degree of alignment in terms of $\langle \cos^2 \theta_{2D} \rangle$ to characterise the molecular alignment distribution, but the knowledge of the whole angular distribution is needed.

Comparison of angular distributions from experiment and simulations

We show a comparison of angular distributions extracted from experiment and from the simulated, 2D projected rotational densities for selected times, starting after the arrival of the second alignment laser pulse in Fig. 8. The angular distributions display rich features, the simplest one being the alignment revival at a delay time of 120.78 ps. For better visibility the angular distri-

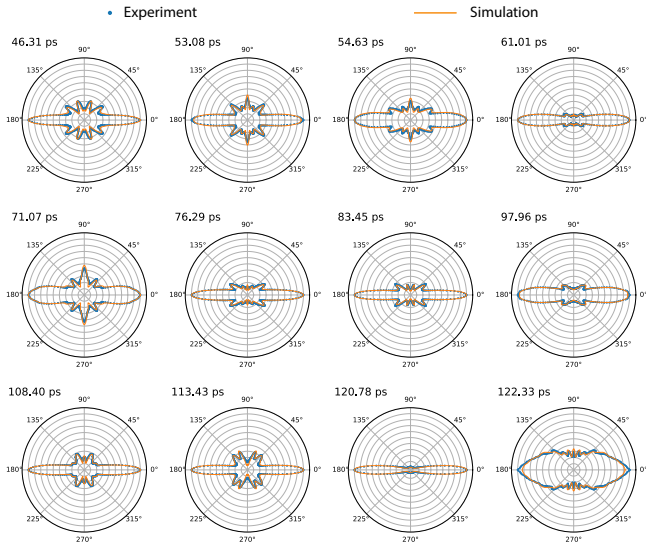


FIG. 8. Comparison of experimental and simulated angular distributions for some selected delay times after the second alignment laser pulse has arrived.

butions have all been scaled up individually to maximise visibility, except for the alignment revival at 120.78 ps.

ANGULAR RESOLUTION

The angular resolution was defined by the radius of the Coulomb channel in the VMI image, at which the angular distribution was extracted, and the number of pixels needed to distinguish two successive maxima or minima. The center of the radial Coulomb channel was at a radius of 46 pixel, which yielded an angle of 1.26° per pixel, corresponding to a limit for the resolution to separate two maxima or minima of 4° . In Fig. 9 a, a O^+ ion momentum distribution recorded at a delay time of 98.5 ps is shown with lines indicating the angles at which maxima in the angular distribution appear. In Fig. 9 b

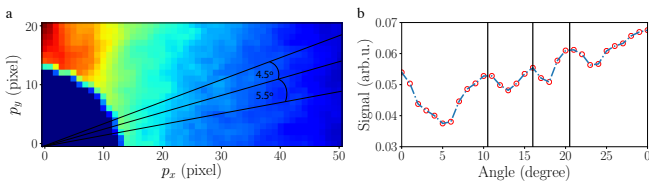


FIG. 9. Determination of angular resolution. **a** Part of the recorded VMI image at a delay time of 98.5 ps is shown with lines indicating the angles at which maxima in the angular distribution were observed. **b** Angular distribution for the same cutout of the VMI image, shown with the position of the maxima indicated by vertical lines. The smallest measured angle between maxima in the angular distribution is 4.5° , close to the angular resolution of 4° .

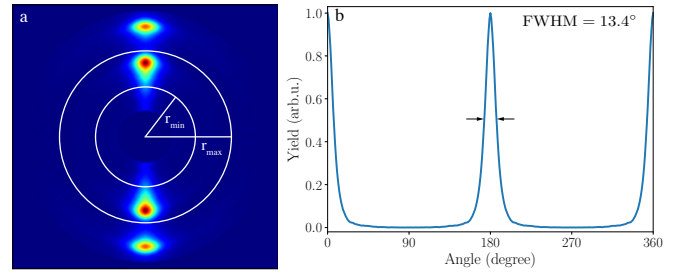


FIG. 10. Observed highest degree of alignment of $\langle \cos^2 \theta_{2D} \rangle = 0.955$. **a** O^+ ion momentum distribution recorded at the alignment revival at a delay time of 120.78 ps. The integration for the calculation of $\langle \cos^2 \theta_{2D} \rangle$ was carried out in the shell between $r_{\min} = 40$ and $r_{\max} = 64$ pixel. **b** Corresponding angular distribution with a full opening angle of $\text{FWHM} = 13.4^\circ$.

the corresponding angular distribution is shown, where the maxima are clearly visible and distinguishable.

HIGHEST OBSERVED DEGREE OF ALIGNMENT

In Fig. 10 a the O^+ ion momentum distribution of the strongest observed field-free alignment is shown. The image was recorded at a delay time of 120.78 ps, which is the alignment revival, one rotational period after the arrival of the second alignment pulse. The degree of alignment was $\langle \cos^2 \theta_{2D} \rangle = 0.96$ as stated in the main text. The value was obtained through integration in the shell between $r_{\min} = 40$ and $r_{\max} = 64$. In Fig. 10 b the corresponding angular distribution is shown, which yielded an opening angle of $\text{FWHM} = 13.4^\circ$.

Acknowledgments

This work has been supported by the Deutsche Forschungsgemeinschaft (DFG) through the priority program ‘‘Quantum Dynamics in Tailored Intense Fields’’ (QUTIF, SPP1840, KU 1527/3, RO4577/4) and by the Clusters of Excellence ‘‘Center for Ultrafast Imaging’’ (CUI, EXC 1074, ID 194651731) and ‘‘Advanced Imaging of Matter’’ (AIM, EXC 2056, ID 390715994) of the Deutsche Forschungsgemeinschaft (DFG), and by the European Research Council under the European Union’s Seventh Framework Programme (FP7/2007-2013) through the Advanced Grant ‘‘DropletControl’’ (ERC-320459-Stapelfeldt) and the Consolidator Grant ‘‘COMOTION’’ (ERC-614507-Küpper).

AUTHOR CONTRIBUTIONS

The project was conceived and coordinated by AR and JK. The experiment was designed by KD, JK, AR; set up by ETK, SR, KD, RRJ, and AR; and performed by ETK, SR, AT, ST, GG, PS, and AR. The data analysis and numerical simulations were performed by ETK, the results from theory and experiment were analyzed by ETK, TM, AT, ST, AR, and JK and discussed with HS and MJJV. The manuscript was prepared by ETK, ST, and JK and discussed by all authors.

COMPETING INTERESTS

The authors declare that they have no competing financial interests.

CORRESPONDENCE

Correspondence and requests for materials should be addressed to Jochen Küpper <jochen.kuepper@cfel.de> and Arnaud Rouzée <rouzee@mbi-berlin.de>.

|| arnaud.rouzee@mbi.de

* jochen.kuepper@cfel.de; <https://www.controlled-molecule-imaging.org>

- [1] A. H. Zewail, “Femtochemistry: Atomic-scale dynamics of the chemical bond,” *J. Phys. Chem. A* **104**, 5660–5694 (2000).
- [2] A. A. Ischenko, P. M. Weber, and R. J. D. Miller, “Capturing chemistry in action with electrons: Realization of atomically resolved reaction dynamics,” *Chem. Rev.* **117**, 11066–11124 (2017).
- [3] K. Ayer, O. M. Yefanov, D. Oberthür, S. Roy-Chowdhury, L. Galli, V. Mariani, S. Basu, J. Coe, C. E. Conrad, R. Fromme, A. Schaffer, K. Dörner, D. James, C. Kupitz, M. Metz, G. Nelson, P. L. Xavier, K. R. Beyerlein, M. Schmidt, I. Sarrou, J. C. H. Spence, U. Weierstall, T. A. White, J.-H. Yang, Y. Zhao, M. Liang, A. Aquila, M. S. Hunter, J. S. Robinson, J. E. Koglin, S. Boutet, P. Fromme, A. Barty, and H. N. Chapman, “Macromolecular diffractive imaging using imperfect crystals,” *Nature* **530**, 202–206 (2016).
- [4] J. Küpper, S. Stern, L. Holmegaard, F. Filsinger, A. Rouzée, A. Rudenko, P. Johnsson, A. V. Martin, M. Adolph, A. Aquila, S. Bajt, A. Barty, C. Bostedt, J. Bozek, C. Caleman, R. Coffee, N. Coppola, T. Delmas, S. Epp, B. Erk, L. Foucar, T. Gorkhover, L. Gumprecht, A. Hartmann, R. Hartmann, G. Hauser, P. Holl, A. Hömke, N. Kimmel, F. Krasniqi, K.-U. Kühnel, J. Maurer, M. Messerschmidt, R. Moshhammer, C. Reich, B. Rudek, R. Santra, I. Schlichting, C. Schmidt, S. Schorb, J. Schulz, H. Soltau, J. C. H. Spence, D. Starodub, L. Strüder, J. Thøgersen, M. J. J. Vrakking, G. Weidenspointner, T. A. White, C. Wunderer, G. Meijer, J. Ullrich, H. Stapelfeldt, D. Rolles, and H. N. Chapman, “X-ray diffraction from isolated and strongly aligned gas-phase molecules with a free-electron laser,” *Phys. Rev. Lett.* **112**, 083002 (2014), arXiv:1307.4577 [physics].
- [5] C. J. Hensley, J. Yang, and M. Centurion, “Imaging of isolated molecules with ultrafast electron pulses,” *Phys. Rev. Lett.* **109**, 133202 (2012).
- [6] K. Pande, C. D. M. Hutchison, G. Groenhof, A. Aquila, J. S. Robinson, J. Tenboer, S. Basu, S. Boutet, D. P. DePonte, M. Liang, T. A. White, N. A. Zatsepin, O. Yefanov, D. Morozov, D. Oberthuer, C. Gati, G. Subramanian, D. James, Y. Zhao, J. Koralek, J. Brayshaw, C. Kupitz, C. Conrad, S. Roy-Chowdhury, J. D. Coe, M. Metz, P. L. Xavier, T. D. Grant, J. E. Koglin, G. Ketawala, R. Fromme, V. Šrajer, R. Henning, J. C. H. Spence, A. Ourmazd, P. Schwander, U. Weierstall, M. Frank, P. Fromme, A. Barty, H. N. Chapman, K. Moffat, J. J. van Thor, and M. Schmidt, “Femtosecond structural dynamics drives the trans/cis isomerization in photoactive yellow protein,” *Science* **352**, 725–729 (2016).
- [7] J. Yang, M. Guehr, X. Shen, R. Li, T. Vecchione, R. Coffee, J. Corbett, A. Fry, N. Hartmann, C. Hast, K. Hegazy, K. Jobe, I. Makasyuk, J. Robinson, M. S. Robinson, S. Vetter, S. Weathersby, C. Yoneda, X. Wang, and M. Centurion, “Diffractive imaging of coherent nuclear motion in isolated molecules,” *Phys. Rev. Lett.* **117**, 153002 (2016).
- [8] P. M. Felker, J. S. Baskin, and A. H. Zewail, “Rephasing of collisionless molecular rotational coherence in large molecules,” *J. Phys. Chem.* **90**, 724–728 (1986).
- [9] F. Rosca-Pruna and M. J. J. Vrakking, “Experimental observation of revival structures in picosecond laser-induced alignment of I₂,” *Phys. Rev. Lett.* **87**, 153902 (2001).
- [10] H. Stapelfeldt and T. Seideman, “Colloquium: Aligning molecules with strong laser pulses,” *Rev. Mod. Phys.* **75**, 543–557 (2003).
- [11] K. Mizuse, K. Kitano, H. Hasegawa, and Y. Ohshima, “Quantum unidirectional rotation directly imaged with molecules,” *Science Advances* **1**, e1400185 (2015).
- [12] P. W. Dooley, I. V. Litvinyuk, K. F. Lee, D. M. Rayner, M. Spanner, D. M. Villeneuve, and P. B. Corkum, “Direct imaging of rotational wave-packet dynamics of diatomic molecules,” *Phys. Rev. A* **68**, 023406 (2003).
- [13] C. Marceau, V. Makhija, D. Platzer, A. Y. Naumov, P. B. Corkum, A. Stolow, D. M. Villeneuve, and P. Hockett, “Molecular frame reconstruction using time-domain photoionization interferometry,” *Phys. Rev. Lett.* **119**, 083401 (2017).
- [14] J. Yang, M. Guehr, T. Vecchione, M. S. Robinson, R. Li, N. Hartmann, X. Shen, R. Coffee, J. Corbett, A. Fry, K. Gaffney, T. Gorkhover, C. Hast, K. Jobe, I. Makasyuk, A. Reid, J. Robinson, S. Vetter, F. Wang, S. Weathersby, C. Yoneda, M. Centurion, and X. Wang, “Diffractive imaging of a rotational wavepacket in nitrogen molecules with femtosecond megaelectronvolt electron pulses,” *Nat. Commun.* **7**, 11232 (2016).
- [15] O. Ghafur, A. Rouzée, A. Gijsbertsen, W. K. Siu, S. Stolte, and M. J. J. Vrakking, “Impulsive orientation and alignment of quantum-state-selected NO molecules,” *Nat. Phys.* **5**, 289–293 (2009).
- [16] S. Trippel, T. Mullins, N. L. M. Müller, J. S. Kienitz, R. González-Férez, and J. Küpper, “Two-state wave packet for strong field-free molecular orientation,” *Phys. Rev. Lett.* **114**, 103003 (2015), arXiv:1409.2836 [physics].

- [17] P. M. Felker, “Rotational coherence spectroscopy: studies of the geometries of large gas-phase species by picosecond time-domain methods,” *J. Phys. Chem.* **96**, 7844–7857 (1992).
- [18] C. Riehn, “High-resolution pump-probe rotational coherence spectroscopy - rotational constants and structure of ground and electronically excited states of large molecular systems,” *Chem. Phys.* **283**, 297–329 (2002).
- [19] K. Lee, D. Villeneuve, P. Corkum, and E. Shapiro, “Phase control of rotational wave packets and quantum information,” *Phys. Rev. Lett.* **93**, 233601 (2004).
- [20] S. Trippel, T. Mullins, N. L. M. Müller, J. S. Kienitz, J. J. Omiste, H. Stapelfeldt, R. González-Férez, and J. Küpper, “Strongly driven quantum pendulum of the carbonyl sulfide molecule,” *Phys. Rev. A* **89**, 051401(R) (2014), arXiv:1401.6897 [quant-ph].
- [21] A. S. Mouritzen and K. Mølmer, “Quantum state tomography of molecular rotation,” *J. Chem. Phys.* **124**, 244311 (2006).
- [22] H. Hasegawa and Y. Ohshima, “Quantum state reconstruction of a rotational wave packet created by a nonresonant intense femtosecond laser field,” *Phys. Rev. Lett.* **101**, 053002 (2008).
- [23] M. Berry, I. Marzoli, and W. Schleich, “Quantum carpets, carpets of light,” *Phys. World* **14**, 39–46 (2001).
- [24] M. Leibscher, I. Averbukh, and H. Rabitz, “Molecular alignment by trains of short laser pulses,” *Phys. Rev. Lett.* **90**, 213001 (2003).
- [25] S. Guérin, A. Rouzée, and E. Hertz, “Ultimate field-free molecular alignment by combined adiabatic-impulsive field design,” *Phys. Rev. A* **77**, 041404 (2008).
- [26] Y.-P. Chang, D. A. Horke, S. Trippel, and J. Küpper, “Spatially-controlled complex molecules and their applications,” *Int. Rev. Phys. Chem.* **34**, 557–590 (2015), arXiv:1505.05632 [physics].
- [27] A. T. J. B. Eppink and D. H. Parker, “Velocity map imaging of ions and electrons using electrostatic lenses: Application in photoelectron and photofragment ion imaging of molecular oxygen,” *Rev. Sci. Instrum.* **68**, 3477–3484 (1997).
- [28] M. Pitzer, M. Kunitski, A. S. Johnson, T. Jahnke, H. Sann, F. Sturm, L. P. H. Schmidt, H. Schmidt-Böcking, R. Dörner, J. Stohner, J. Kiedrowski, M. Reggelin, S. Marquardt, A. Schießer, R. Berger, and M. S. Schöffler, “Direct determination of absolute molecular stereochemistry in gas phase by coulomb explosion imaging,” *Science* **341**, 1096–1100 (2013).
- [29] L. Christensen, J. H. Nielsen, C. B. Brandt, C. B. Madsen, L. B. Madsen, C. S. Slater, A. Lauer, M. Brouard, M. P. Johansson, B. Shepperson, and H. Stapelfeldt, “Dynamic stark control of torsional motion by a pair of laser pulses,” *Phys. Rev. Lett.* **113**, 073005 (2014).
- [30] A. Owens, A. Yachmenev, S. N. Yurchenko, and J. Küpper, “Climbing the Rotational Ladder to Chirality,” *Phys. Rev. Lett.* **121**, 193201 (2018), arXiv:1802.07803 [physics].
- [31] E. W. Kuipers, M. G. Tenner, A. Kleyn, and S. Stolte, “Observation of steric effects in gas-surface scattering,” *Nature* **334**, 420–422 (1988).
- [32] T. P. Rakitzis, A. J. van den Brom, and M. H. M. Janssen, “Directional dynamics in the photodissociation of oriented molecules,” *Science* **303**, 1852–1854 (2004).
- [33] J. Itatani, J. Levesque, D. Zeidler, H. Niikura, H. Pépin, J. C. Kieffer, P. B. Corkum, and D. M. Villeneuve, “Tomographic imaging of molecular orbitals,” *Nature* **432**, 867–871 (2004).
- [34] L. Holmegaard, J. L. Hansen, L. Kalhøj, S. L. Kragh, H. Stapelfeldt, F. Filsinger, J. Küpper, G. Meijer, D. Dimitrovski, M. Abu-samha, C. P. J. Martiny, and L. B. Madsen, “Photoelectron angular distributions from strong-field ionization of oriented molecules,” *Nat. Phys.* **6**, 428 (2010), arXiv:1003.4634 [physics].
- [35] F. Filsinger, G. Meijer, H. Stapelfeldt, H. Chapman, and J. Küpper, “State- and conformer-selected beams of aligned and oriented molecules for ultrafast diffraction studies,” *Phys. Chem. Chem. Phys.* **13**, 2076–2087 (2011), arXiv:1009.0871 [physics].
- [36] S. J. Weber, M. Oppermann, and J. P. Marangos, “Role of rotational wave packets in strong field experiments,” *Phys. Rev. Lett.* **111**, 263601 (2013).
- [37] M. G. Pullen, B. Wolter, A.-T. Le, M. Baudisch, M. Hemmer, A. Senftleben, C. D. Schroter, J. Ullrich, R. Moshhammer, C. D. Lin, and J. Biegert, “Imaging an aligned polyatomic molecule with laser-induced electron diffraction,” *Nat. Commun.* **6**, 7262 (2015).
- [38] A. Barty, J. Küpper, and H. N. Chapman, “Molecular imaging using x-ray free-electron lasers,” *Annu. Rev. Phys. Chem.* **64**, 415–435 (2013).
- [39] M. Hillenkamp, S. Keinan, and U. Even, “Condensation limited cooling in supersonic expansions,” *J. Chem. Phys.* **118**, 8699–8705 (2003).
- [40] J. H. Nielsen, P. Simesen, C. Z. Bisgaard, H. Stapelfeldt, F. Filsinger, B. Friedrich, G. Meijer, and J. Küpper, “Stark-selected beam of ground-state OCS molecules characterized by revivals of impulsive alignment,” *Phys. Chem. Chem. Phys.* **13**, 18971–18975 (2011), arXiv:1105.2413 [physics].